Bachelor's thesis

Constraints of supersymmetric models with LHC data and direct search for dark matter

Einschränkung supersymmetrischer Modelle mit LHC-Daten und direkter Suche nach Dunkler Materie

Mirko Gabski

Münster, July 25, 2013

Supervisor & 1. Examiner :	Prof. Dr. Michael Klasen
2. Examiner :	Jun. Prof. Dr. Anna Kulesza

Contents

1 Introduction

The **S**tandard **M**odel (SM) of particle physics describes three of four fundamental interaction, electromagnetism, weak and strong interactions via a quantum field formalism. By using space-time and internal gauge symmetries the SM leads to very precise predictions. But there are still some phenomena which can not be explained with the SM. Examples for those phenomena are dark matter and dark energy, the asymmetry between matter and antimatter in the universe, the hierarchy and the fine-tuning problem[1][3].
Since symmetry is a very strong tool which already lead to the SM, it seems to be reasonable to assume further symmetries to extend the SM to get rid of those problems. The **su**per**sy**mmetry (**SUSY**) is one possible extension of the SM by demanding further symmetries. SUSY assumes a symmetry between bosonic and leptonic particles and predicts fermionic (bosonic) hypothetical supersymmetric partners for the SM bosons (fermions). For example the dark matter problem could be solved since SUSY predicts a weakly interacting stable particle which would serve as a candidate for dark matter. On the other hand there is a need for more parameters(e.g. SUSY-particle masses,couplings,...) which can be reduced to just four parameters and a relativ sign by using the mSUGRA SUSY breaking scenario. But even those four parameters are unknown and therefore are treated as arbitrary[3].
Because of this arbitrariness it seems to be a very good idea to constraint these parameters by as much experimental data as possibly. This will be done during this thesis by comparing the theoretical results from SUSY calculations for different parameter sets with the experimental data.
First there will be a brief explaination of the SM, SUSY und Dark Matter. Followed by a short introduction of the used constraints. Then these constraints will be calculated for different mSUGRA input parameters, first for fixed parameter steps to achieve an overview and second via a Markov Chain Monte Carlo algorithm to find parameter sets which would fulfil the constraints.

2 Theoretical background

2.1 Standard Model

This section is based on Ref. [1].

The **S**tandard **M**odel (**SM**) of particle physics is a quantum field theory which describes three of the four fundamental interaction in nature by using fields. Since it is a quantum theory these fields can only be varied in discrete packets. Those packets can be interpreted as particles. The SM decsribes all known particles and their interaction, except gravity, very percisely and even includes special relativity, but one although has to notice that the SM has 18 free parameters (fermion masses,coupling constants,...), which have to be determined experimentally.

2.1.1 Particle content

The SM contains 37 particles, 6 quarks, 6 leptons, 12 gauge bosons and the Higgs boson, furthermore there are the corresponding antiquarks and antileptons. The particle content of the SM is shown in Tab. 1.

Table 1: Particle content of the SM.

generation /family	1.	2.	3.	gauge boson	Higgs boson
quarks	u	c	t	γ	h
	d	s	b	g	
leptons	e^-	μ^-	τ^-	Z	
	ν_e	ν_μ	ν_τ	$W^\pm$	

At first the particles are arranged into fermions (spin 1/2) and bosons (spin 0,1). The bosons are classified into gauge bosons (spin 1) and the higgs boson (spin 0). The fermions are classified into particle that 'feel' the strong interaction the so-called baryons and particles that do not the so called leptons. Furthermore quarks and leptons are grouped into three generations or families with increasing particle mass and different flavors (e.g. strangeness, topness, L_e, ...). The rest of the particles characteristics (e.g Charge, color-charge, ...) stay the same. This means that for instance electrons e^-, muons μ^- and tauons τ^- have the same electric charge and therefore would behave similar in a magnetic field.

By now there are pairs of two baryons and pairs of two leptons for each generation. Each particle of one pair behaves different under a certain interaction. The quarks can be distinguished into up-type quarks (u, c, t) and down-type quarks (d, s, b) and the leptons can be distinguished into charged leptons (e^-, μ^-, τ^-) and neutral so-called neutrinos $(\nu_e, \nu_\mu, \mu_\tau)$. One great difference between quarks and leptons is the so-called confinement, which means that quarks cannot be isolated, respective that observed particles have to be color neutral or white (red+green+blue=white or color+anticolor=white). This is due to the fact that simulations have shown that color-charged particles gain energy when their distance towards each other is increased. This means that at a certain distance it is energetically easier to create a quark/antiquark pair, which leads to two color neutral particles, than separating two color-charged particles[2].

To understand this seperation into different groups one has to take a closer look at the particle properties or quantum numbers. Tab. 2 shows the particles and their quantum numbers, where e is the elementary charge, Q the particles charge, B the baryon number, L the lepton number, I_3 the third component of the isospin, C the charmness, S the strangeness, T the topness, B' the bottomness and $L_{e,\mu\tau}$ the leptonic flavor.

Table 2: Quantum numbers of the SM particles.

Particle	Charge Q	Baryon number B	Lepton number L	Flavor	
u	$2e/3$	$1/3$	0	$I_3 = 1/2$	quark flavor
d	$-e/3$	$1/3$	0	$I_3 = -1/2$	
c	$2e/3$	$1/3$	0	$I_3 = 0, C = 1$	
s	$-e/3$	$1/3$	0	$I_3 = 0, S = -1$	
t	$2e/3$	$1/3$	0	$I_3 = 0, T = 1$	
b	$-e/3$	$1/3$	0	$I_3 = 0, B' = -1$	
e^-	-e	0	1	$L_e = 1$	leptonic flavor
μ^-	-e	0	1	$L_\mu = 1$	
τ^-	-e	0	1	$L_\tau = 1$	
ν_e	0	0	1	$L_e = 1$	
ν_μ	0	0	1	$L_\mu = 1$	
ν_τ	0	0	1	$L_\tau = 1$	

To get the corresponding antiparticles one simply has to the change the signs for all these quantum numbers. One has to notice that each particle has its mass which is the same for particle and antiparticle.
There are so called majorana particles, which are particle whose quantum numbers are the same for particle and antiparticle. But this could only be the case for neutral particles, for example neutrinos.
Furthermore there is the leptonic flavor which is connected to the leptons generation. It is important to know thaht those quantum numbers are conserved during strong and electromagnetic interactions, while the flavors can be violated during weak interaction.

One important fact about the weak interaction is that it distinguishes between particles of different chirality. Chirality or handedness is defined by via the particles spin and its momentum. If the spin is parallel aligned to the particles momentum, the particle is called right-handed (index R) and if the spin is antiparallel aligned to the particles momentum it is called left-handed (index L). One has to notice that no right-handed neutrinos have observed yet.
To describe the weak interaction one can now define the weak hypercharge $Y_\mathrm{W} = 2(Q - T_3)$ with the third component of the weak isospin T_3, which is a conserved quantities of the weak interaction. Tab. 3 shows the third component of the weak isospin and the weak hypercharge for the SM particles.

Table 3: Weak Isospin and weak hypercharge.

particle	3rd component of the Weak isospin T_3	Weak hypercharge Y_W
u_L, c_L, t_L	1/2	1/3
d_L, s_L, b_L	-1/2	1/3
e_L, μ_L, τ_L	1/2	-1
ν_e, ν_μ, ν_τ	-1/2	-1
u_R, c_R, t_R	0	4/3
d_R, s_R, b_R	0	-2/3
e_R, μ_R, τ_R	0	-2

2.1.2 Interactions

Each interaction is represented by a certain gauge group at which the force-carriers or gauge bosons are represented by the generators of the corresponding gauge group. Interactions and their corresponding groups and gauge bosons are shown in Tab. 4.

Table 4: Interactions and their corresponding gauge groups and gauge bosons.

interaction	gauge group	number of generators	gauge bosons
strong interaction	SU(3)	8	gluon g
weak interaction	SU(2)	3	Z-, $W^{\pm}$-boson
electromagnetic interaction	U(1)	1	photon γ

The strong interaction is represented by the SU(3) gauge group and is mediated by gluons. Since gluons are color-charged they are not only able to mediate the strong interaction between color-charged particles but although between each other, this behavior is called selfinteraction. The strong interaction is caused by gluon mediated color changing.
The weak interaction is represented by the SU(2) gauge group and is mediated by Z- and $W^{\pm}$-bosons. It is the only SM interaction that is able to change a particles flavor (e.g. $d \longrightarrow u + e^{-} + \bar{\nu_e}$).
The electromagnetic interaction is represented by the U(1) gauge group and is mediated by photons.

2.1.3 Electroweak Symmetry Breaking and Higgs Mechanism

At the so-called electroweak scale the electromagnetic and the weak interaction unify to the electroweak interaction. The electroweak gauge bosons are the B^0, W^0, W^1 and W^2 boson. The transition from electroweak interaction to electromagnetic and weak interaction is called symmetry breaking.
Usually the SM particles are assumed to be massless at energies higher than the electroweak scale, since one could not easily add a mass term to the SM Lagrangian without affecting its lorentz invariance. Therefore a special mass generating mechanism is needed, the so-called Higgs mechanism, which introduces the scalar Higgs field to the SM. The Higgs field causes the electrõweak symmetry breaking, during this symmetry breaking the fermionic particles gain their mass and the neutral B^0- and W^0-boson mix to the massless photon γ and the massive Z-boson and the charged W^1- and W^2-bosons mix to the massive W^+- and W^--bosons.

2.2 Supersymmetry

This section is based on Ref. [3].

2.2.1 Shortcomings of the Standard Model

Even though the SM has tremendous predictive power, there are still problems and open questions. For instance: The SM does not predict dark matter and dark energy. Furthermore the SM does not include gravity nor it explains the asymmetry between matter and antimatter in the universe. Then there are the fine-tuning problem and the hierarchy problem. Due to this it seems that a new theory or at least an extension of the SM is needed. Since symmetries lead to the SM it might be a good idea to use further symmetries to expand the SM.

2.2.2 From SM to SUSY

We will take a closer look at one of this problems. Because of the Higgs bosons scalar nature the correction to the Higgs bare mass depend quadratically on the scale up to which one assumes the SM to be valid, usually the Planck scale. This makes the whole SM sensitive to this scale. Either one accepts the fact that the Higgs bare mass has to be chosen very carefully, avoid theories which use the Higgs mechanism or one finds a way to cancel out the quadratically dependence with the scale.
If one now assumes a massive fermion, whose quantum numbers are similar to those of the SM vector bosons it would contribute to the Higgs mass correction term quadratically with the scale, but due to its spin, with an opposite sign, so the quadratic dependence cancels out. So this might be the symmetry we are looking for: a symmetry which connects SM bosons to fermionic particles with the same quantum numbers. Same for the SM fermions which should be somehow connected to some bosons which have the same quantum numbers.
This is the so called **su**per**sy**mmetry or short SUSY. So for each boson (fermion) there should be a supersymmetric fermionic (bosonic) partner with the same quantum numbers. Since for example no bosonic electrons or massless spin 1/2 particles are discovered, one can see that SUSY cannot be an exact symmetry. Due to experimental Data it seems that SUSY particle have masses around or higher than 1 TeV/c^2 for most SUSY particles.

2.2.3 Minimal Supersymmetric Standard Model

As one can guess from the name the **M**inimal **S**upersymmetric **S**tandard **M**odel **MSSM** is the minimal possible realisation of a supersymmertic extension of the SM. It contains one supersymmetric partner for each SM particle and the interactions remain the same. The superpartners of the SM fermions are called sfermions (e.g. selectron, up-squark,...) and the SM bosons are extended with the suffix '-ino' (e.g. gluino, Higgsino,...). All superparticles symbols are marked with a tilde (e.g.$\tilde{e}, \tilde{\nu}_e, \tilde{g}, ...$). The particle content of the MSSM can be listed very easily, except for the fact that now two Higgs doublets are needed to generate every particles mass: one up-type doublet (H_u^+, H_u^0) and one down-type doublet (H_d^0, H_d^-), each consisting of one neutral and one charged Higgs. The particle content of the MSSM is shown in Tab. 5. The quantum numbers are not mentioned here, since they are already known from the SM. The superpartner masses are generated via the Higgs mechanism too.

Table 5: Particle content of the MSSM.

	SM-particle	superpartner
$U(1)_Y$	B^0	$\tilde{B}^0$
$SU(2)_L$	W^0, W^1, W^2	$\tilde{W}^0, \tilde{W}^1, \tilde{W}^2$
$SU(3)_C$	g	$\tilde{g}$
leptonen/ sleptonen	e, μ, τ ν_e, ν_μ, ν_τ	$\tilde{e}, \tilde{\mu}, \tilde{\tau}$ $\tilde{\nu}_e, \tilde{\nu}_\mu, \tilde{\nu}_\tau$
quarks/ squarks	u, c, t d, s, b	$\tilde{u}, \tilde{c}, \tilde{t}$ $\tilde{d}, \tilde{s}, \tilde{b}$

Similar to the mixing of the B and W gauge eigenstates to the massless photon γ and the massive mass eigenstate Z and $W^{\pm}$ bosons in the electroweak gauge sector of the SM, occurs a mixing of the eigenstates Wino, Bino and Higgsino to the mass eigenstate neutralinos $\tilde{N}_1^0, \tilde{N}_2^0, \tilde{N}_3^0, \tilde{N}_4^0$ (or $\tilde{\chi}_1^0, \tilde{\chi}_2^0, \tilde{\chi}_3^0, \tilde{\chi}_4^0$) and charginos $\tilde{\chi}_1^{\pm}, \tilde{\chi}_2^{\pm}$. As one can guess from the names the neutralinos are electrically neutral and the charginos are electrically charged.

One important new quantum number of the MSSM is the so-called R-parity $P_R = (-1)^{3B+L+2s}$, where B is the baryon number, L is the lepton number and s the particles spin. All SM particles have the R-parity $P_R = 1$ and the superpartners $P_R = -1$. This leads to the fact that the lightest supersymmetric particle, the so-called LSP, has to be stable, since the R-parity is a conserved quantum number.
Depending on its properties the LSP might be a candidate for cold dark matter. Therefore it should be neutral, massive and weakly interacting. Which means it would only interact with matter via gravitational and weak interaction.

2.2.4 Breaking scenario & mSUGRA

Since SUSY is not an exact symmetry a breaking mechanism is needed. This can be done via a term in the MSSM Lagrangian or via spontaneous symmetry breaking similar to the electroweak sector. Since the breaking mechanism is unknown, one introduces a phenomenologically breaking term into the MSSM Lagrangian. This Lagrangian should be soft and of positive mass dimension.
This ensures the cancellation of the quadratic divergence of scalar mass term. The scale of the soft SUSY breaking should not be much larger then 1 TeV to avoid the fine-tuning problem. After introducing this breaking term the MSSM ends up with 105 extra free parameter which add to the 18 of the SM. This leads to a huge arbitrariness in the MSSM. Furthermore it is technically unfeasible to scan a parameter space with over 100 dimensions.
One of the most common breaking scenarios is the so-called **m**inimal **su**per**gr**vity (**mSUGRA**). mSUGRA is the minimal realisation of this supergravitational symmetry breaking and mediates the SUSY breaking via a hidden sector which is connected to the visible sector via gravitational interaction. mSUGRA generates the needed soft breaking term naturally.
There are two important assumptions. First that all (squark and sfermion) mass matrices are proportional the unit matrices, to avoid further flavor violation, and second that the triple scalar couplings are proportional to the Yukawa couplings. Furthermore no new complex phases are introduced. If

one now assumes that masses and couplings unify at a high energy scale, there are only four parameters left. The mass of the spin 1/2 SUSY particles $m_{1/2}$, the mass of the spin 0 SUSY particles m_0, the trilinear coupling A_0 and the mixing angle of the two neutral Higgs boson vacuum expectation values $\tan(\beta) = \langle H_u^0 \rangle / \langle H_d^0 \rangle$. And there is although the relative sign for μ in the Higgs potential.
A four dimensional parameter space is much easier to analyse than one with over 100 dimensions. The only thing one has to do now is to calculate back the unified masses and couplings to get the mass spectrum of the SUSY particles at the electroweak scale. This is done by using so-called renormalization group equations (**RGE**s).

2.3 Dark Matter

This subsection is based on Ref. [5].

Around 1970 Vera C. Rubin and W. Kent Ford, Jr. observed that the rotation velocity of stars within galaxies behaves differently than expected. From the visible matter inside a galaxy one would expect a decreasing rotation velocity with increasing distance from the galactic center, but a nearly constant rotation velocity is observed[4]. To explain this one assume a halo of non-visible matter, so-called dark matter. Since dark matter is not visible it does not produce, or maybe even interact with any form of electromagnetic radiation.
One possible candidate for dark matter are so-called **w**eakly **i**nteracting **m**assive **p**articles or short **WIMP**s. WIMPs should be electrically neutral, massive and stable on a cosmoligical timescale. The only WIMP candidates within the SM are the neutrinos, which only interact via gravity and weak interaction. But due to their very small masses the neutrinos would move with velocities close the speed of light and are therefore not able to form halos. This type of fast moving WIMPs is called hot dark matter.
We are looking for slow moving dark matter particles, so called cold dark matter. The MSSM provides a possible cold dark matter candidate: the neutralino, which like neutrinos only interacts via gravity and weak interaction. Depending on the chosen MSSM input parameters the lightest neutralino might be the LSP and therefore stable, so that all SUSY particles should have been decayed into neutralinos over time.
This may explain the abcense of SUSY particles and provide a sufficent relic density. Furthermore, since the neutralino mass is much greater than the neutrino mass, the neutralino might move slow enough to form halos.

2.4 Markov Chain Monte Carlo

This section is based on Ref. [7].

The Markov Chain Monte Carlo algorithm in general is used to find the minimum of a function and explore the region around this minimum. During this thesis the Metropolis algorithm is used and will be explained in the way it is used. The Metropolis algorithm uses a sequence of points $P_0 \longrightarrow P_1 \longrightarrow P_2 \longrightarrow ...$, with a transition probability to get from the point P_i to the point P_{i+1}. During this thesis the whole parameter space provides possible points and one has to decide which of those points should be chosen.

At first one defines a likelihood function $L = \exp(\chi^2/2)$, where χ^2 relates the probed constraint and will be explained later (see section 3.2).
The first point $P_0(x_1, x_2, ..., x_n)$, where $x_1, x_2, ...x_n$ are the coordinates of the point within the parameter space, is chosen randomly under the condition that $L(P_0) > 0$.
From now on the procedure is the same for every new point:

- **First:** A new point is generated by making a random step in the parameter space. This is done by generating a random step Δx_j for each parameter with $\Delta x_j \in [0 : \Delta x_j^{\max} = x_j^{\max} - x_j^{\min}]$, where $\Delta x_j^{\max}$ is the maximum step width, $x_j^{\min}$ is the minimal and $x_j^{\max}$ the maximum value for this parameter, and adding the step with a random sign to the coordinate of the previous point: $P_i(x_1, x_2, ..., x_n) \longrightarrow P_{i+1}(x_1 + \Delta x_1, x_2 + \Delta x_2, ..., x_n + \Delta x_n)$.
  If $x_j + \Delta x_j$ is greater than $x_j^{\max}$ one subtracts $x_j^{\max} - x_j^{\min}$ from $x_j + \Delta x_j$ and if $x_j + \Delta x_j$ is less than $x_j^{\min}$ one adds $x_j^{\max} - x_j^{\min}$ to $x_j + \Delta x_j$, so that the new point is within the valid parameter space.

- **Second:** One checks if the new point is accepted. Therefore one defines an acceptance probability $A(P_{i+1}, P_i)$, where $A(P_{i+1}, P_i) = 1$ for $L(P_{i+1}) > L(P_i)$ and $A(P_{i+1}, P_i) = L(P_i)/L(P_{i+1})$ for $L(P_{i+1}) \leq L(P_i)$. Due to this points with a higher likelihood than the previous one are always taken.
  To decide if a point of a lesser likelihood is accepted one generates a random number $n \in [0; 1]$ and compares it with the acceptance probability. The new point is accepted if the random n is lesser than $A(P_{i+1}, P_i) = L(P_i)/L(P_{i+1})$, otherwise it is rejected and a new random point P_{i+1} is generated as described above and then tested for acceptance.

It has been shown that the fastest exploration of the parameter space happens if about 1/4 of the generated points is accepted. To adjust the acceptance rate, which is defined as the number of accepted points devided by the number of all generated points, one decreases the maximum step width by the factor 2 if the acceptance rate is below 1/4 and increases it by the factor 2 if it is above 1/4.
If the adjusted maximum step width is greater than the initial maximum step width or becomes zero, it is reseted to the initial value.

3 Computation and Results

3.1 Used Software

During this computations 'SPheno'[8][9] is used as a mass spectrum calculator. 'SPheno' calculates the SUSY particles masses and other low energy properties, such as decays and the anomalous magnetic moment of the muon from the MSSM input parameters. 'micrOMEGAs'[10] is used to compute dark matter properties, such as the relic density or the cold dark matter nucleon cross section, from the MSSM parameters.
Furthermore self-written python code is used to for the fixed step and Markov Chain calculations. It uses the MSSM parameters and the constraints as input for the calculations and passes the MSSM input to 'SPheno' and 'micrOMEGAs', reads the needed data from the 'SPheno' and 'micrOMEGAs' output an computes a deviation of the constraints.
The fixed step calculation is simply done by using for-loops for the masses m_0 and $m_{1/2}$ and leaving $\tan(\beta)$ and A_0 fixed. The Markov Chain calculation is done as described in section2.4.

3.2 Constraints

The used contraints and their values are shown in Tab. 6.

Table 6: constrains used for computing[11].

Constraint	Data	Ref.
Ωh^2	0.113 ± 0.004	[12]
$b \longrightarrow X_S \gamma$	$(3.55 \pm 0.24) \cdot 10^{-4}$	[13]
$B_u \longrightarrow \tau \nu$	$(1.68 \pm 0.31) \cdot 10^{-4}$	[13]
$B_S^0 \longrightarrow \mu^+ \mu^-$	$< (4.5 \pm 0.2) \cdot 10^{-9}$	[14]
Δa_μ	$(3.02 \pm 1.24) \cdot 10^{-9}$	[15]
m_h	$> (114.4 \pm 0.5)$ GeV	[16]
m_A	$> (480 \pm 50)$ GeV	[17],[18]
$\sigma_{\chi N}$	$< (2 \pm 1) \cdot 10^{-8}$ pb	[19]

- Ωh^2**:**
  The first constraint is the relic density Ωh^2 as determined by the Wilkinson Microwave Anisotropy Probe (WMAP)[12]. The relic density can be calculated via:

$$\Omega h^2 = \frac{8\pi\, G_{\mathrm{N}}\, n_0\, m_{\tilde{\chi}}}{3H_0^2}, \tag{1}$$

  where G_{N} is the gravitational constant, H_0 is the Hubble expansion rate in units of $100\frac{\mathrm{km}}{\mathrm{s{\cdot}Mpc}}$, $m_{\tilde{\chi}}$ is the WIMP mass, in this case the lightest neutralino mass, and n_0 is the present number density. n_0 can be received by solving the Boltzmann equation:

$$\frac{\mathrm{d}n_{\tilde{\chi}}}{\mathrm{d}t} = -3Hn_{\tilde{\chi}} - \langle\sigma_{\mathrm{ann}}\nu\rangle(n_{\tilde{\chi}}^2 - n_{\mathrm{eq}}^2), \tag{2}$$

  where H is the time independent Hubble expansion rate, n_{eq}^2 is the number of relic particles in thermal equilibrium and $\langle\sigma_{\mathrm{ann}}\nu\rangle$ is the thermally averaged annihilation cross section[22]. Therefore the relic density should be proportional to the neutralino mass.

- $b \longrightarrow X_S\gamma$**:**
  The second constraint is the branching ratio of the bottom quark decay into a final state with strangeness $s = -1$ and a photon: $b \longrightarrow X_S\gamma$. It is the average of the measurements from the experiments BaBar, Belle and the CLEO detector at the CSER[12]. This branching ratio should be the SM value plus some SUSY correction which arise from charged Higgs and chargino loop contributions and should be therefore be sensitive to their masses[20].

- $B_u \longrightarrow \tau\nu$**:**
  The third constraint is the branching ratio of the B-meson decay into a tau-lepton and a neutrino: $B_u \longrightarrow \tau\nu$. It is the average of the measurements from the experiments BaBar, Belle and the CLEO detector at the CSER[12]. This branching ratio receives SUSY corrections at tree level from the charged Higgs and is therefore sensitive to the charged Higgs mass.

- $B_S^0 \longrightarrow \mu^+\mu^-$**:**
  The fourth constraint is the upper limit for the branching ratio of the B_S^0-meson into a muon anti-muon pair: $B_S^0 \longrightarrow \mu^+\mu^-$. It is

determined by the LHCb experiment at the LHC[14]. This branching ratio should be suppressed by the pseudo-scalar Higgs mass m_A($BR(B_S^0 \longrightarrow \mu^+\mu^-.) \propto \frac{1}{m_A^4}$)[23].

- Δa_μ**:**
  The fifth constraint is the anomalous magnetic muon moment Δa_μ as determined by the E821 experiment at BNL[15]. The anomalous magnetic muon moment receives a SUSY contribution which should decrease for higher mass parameters[25].

- m_h**:**
  The sixth constraint is the lower limits for the MSSM Higgs mass m_h as determined by the experiments ALEPH, DELPHI, L3 and OPAL at the LEP[16]. The Higgs mass m_h calculates easily as mentioned in Ref. [3] via:

$$m_h = \frac{1}{2}\left(m_A^2 + m_Z^2 - \sqrt{(m_A^2 - m_Z^2)^2 + m_A m_Z \sin^2(2\beta)}\right). \quad (3)$$

- m_A
  The seventh constraint is the lower limits for the pseudo-scalar Higgs mass m_A as determined by the ATLAS and CMS experiment at the LHC via decay into tau pairs[17][18]. It is proportional to m_0 and $m_{1/2}$[3].

- $\sigma_{\chi N}$
  The eighth constraint is the upper limit for the string independent cold dark matter nucleon cross section $\sigma_{\chi N}$ as determined by the XENON100 experiment[19]. It depends on the WIMP mass as shown in Fig.5 in Ref. [19].

To combine these constraints one defines a deviation from the expected value analogous to Ref. [11] via :

$$\chi^2 = \sum_\alpha \frac{(\alpha_{\text{calc}} - \alpha_{\text{exp}})^2}{\sigma_\alpha^2}, \quad (4)$$

where α_{calc} is the computed value for the constraint α, α_{exp} is the expected value for this constraint from Tab. 6 and σ_α the corresponding uncertainty. Furthermore one defines the deviation from the minimal χ^2 as:

$$\Delta\chi^2 = \chi^2 - \chi^2_{\text{min}}. \quad (5)$$

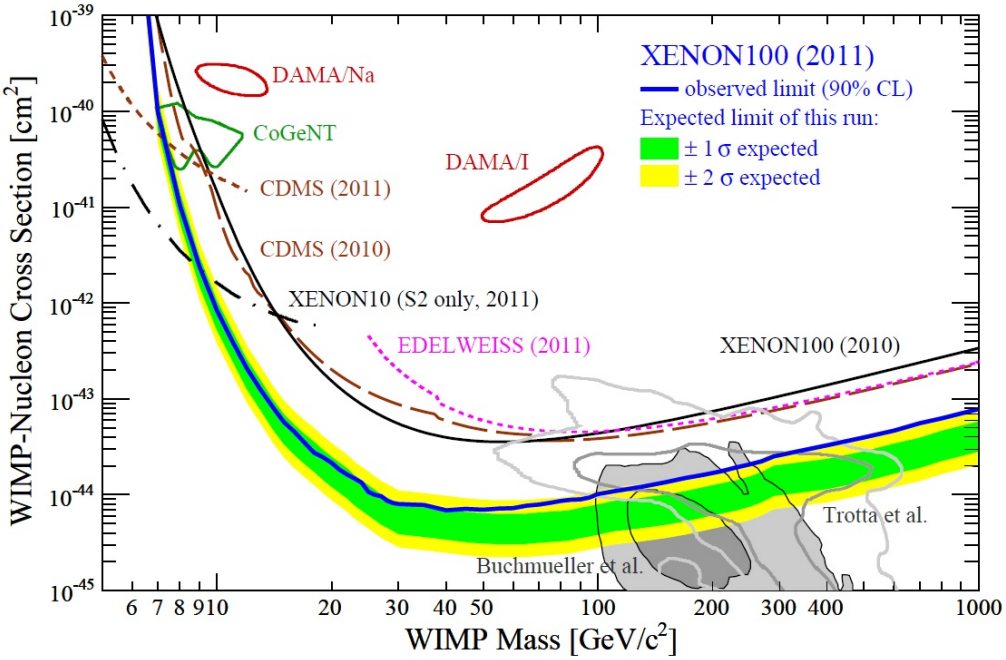

Figure 1: Spin independent WIMP nucleon cross section,Ref.[19]

3.3 Computation with fixed mass steps for fixed $\tan(\beta)$ and A_0.

All calculations are done for $\mu > 0$. This choice is motivated by the anomalous magnetic moment of the muon[26]. The first computations where done for fixed steps for m_0 and $m_{1/2}$ and fixed values for $\tan(\beta)$ and A_0. An example for those calculations is done for $\tan(\beta) = 30$ and $A_0 = 500$ and m_0 and $m_{1/2}$ from 30 GeV to 3000 GeV, with steps of 30 GeV for both masses: $\Delta m_0 = \Delta m_{1/2} = 30$ GeV. The Figures 2 to 9 show the results of this calculations for the individual constraints. Fig. 10 shows the deviation $\Delta\chi^2$ of χ^2 from the minimal χ^2 of this calculation. The upper left corner in Fig. 2 and 9 is left out, since the LSP would be charged for this parameter sets. In Fig. 3,4,5,6,7 and 8 the regions where the SPheno aborded the calculation, due to problems in different loop calculations, are left out. This of course leads to combination of the omitted regions in Fig. 10.

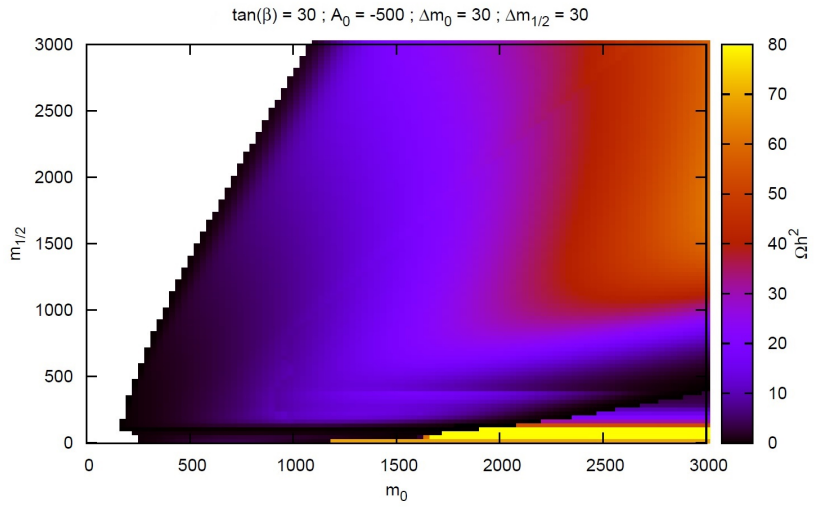

Figure 2: Ωh^2 for fixed $\tan(\beta) = 30$ and $A_0 = -500$ and fixed steps for m_0 and $m_{1/2}$.

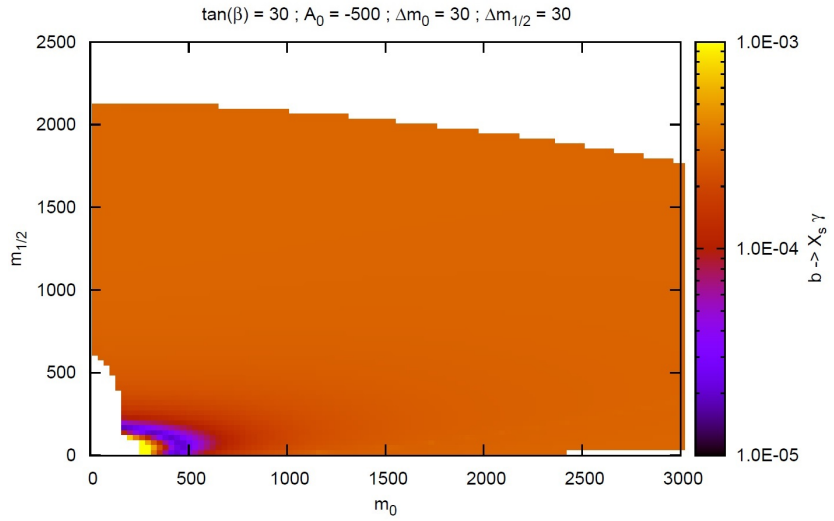

Figure 3: $b \longrightarrow X_S\gamma$ for fixed $\tan(\beta) = 30$ and $A_0 = -500$ and fixed steps for m_0 and $m_{1/2}$.

Fig. 2 shows the calculated relic density Ωh^2 for $\tan(\beta) = 30$ and $A_0 = -500$ and steps of 30 GeV for m_0 and $m_{1/2}$ from 30 to 3000 GeV. The relic density increases for increasing m_0 and $m_{1/2}$, expect for small $m_{1/2}$ below around 200

GeV. In this region happens a very rapid increase of the relic density towards smaller $_{1/2}$. The expected value $\Omega h^2 = (0.113 \pm 0.004)$ is represented by the nearly black colored area on the edge to the charged LSP region in the upper left corner and at masses for $m_{1/2}$ below 500 GeV in Fig. 2.

Fig. 3 shows the calculated branching ratio of the $b \longrightarrow X_S\gamma$ decay for $\tan(\beta) = 30$ and $A_0 = -500$ and steps of 30 GeV for m_0 and $m_{1/2}$ from 30 to 3000 GeV. For m_0 above 400 GeV and $m_{1/2}$ above 700 GeV the branching ratio remains nearly constant. Below this value, there is at first a decrease(violet area) followed by an increase of the branching ratio for smaller m_0 and $m_{1/2}$. This behaviour matches with the expectation that the loop contributions should be less for higher chargino and charged Higgs masses, which both scale with the pseudo-scalar Higgs mass, which itself scales with m_0 and $m_{1/2}$. There should be bigger contributions for low m_0 and $m_{1/2}$, while the contributions decrease for increasing masses. The expected value $b \longrightarrow X_S\gamma = (3.55 \pm 0.24) \cdot 10^{-4}$ is represented by the very small yellow-orange region in the lower left corner ($m_0 < 400$ GeV, $m_{1/2} < 200$ GeV) in Fig. 3.

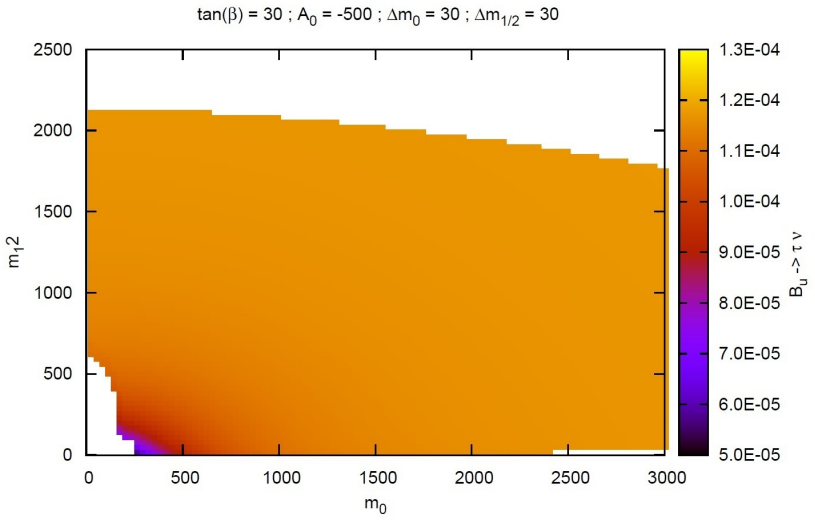

Figure 4: $B_u \longrightarrow \tau\nu$ for fixed $\tan(\beta) = 30$ and $A_0 = -500$ and fixed steps for m_0 and $m_{1/2}$.

Fig. 4 shows the calculated branching ratio of the $B_u \longrightarrow \tau\nu$ decay for $\tan(\beta) = 30$ and $A_0 = -500$ and steps of 30 GeV for m_0 and $m_{1/2}$ from 30 to 3000 GeV. Beginning from small m_0 and $m_{1/2}$ the branching ratio

decreases until m_0 around 350 GeV and $m_{1/2}$ around 700 GeV. From this on the branching ratio remains nearly constant. The same as said above is valid for this branching ratio, great loop contributions for low m_0 and $m_{1/2}$, while the contributions decrease for high m_0 and $m_{1/2}$. The expected value $B_u \longrightarrow \tau\nu = (1.68 \pm 0.31) \cdot 10^{-4}$ is not represented in Fig. 4, since the plots scale ends at around $1.2 \cdot 10^{-4}$. But the great orange area is quite close to the lower limit for $B_u \longrightarrow \tau\nu$, which is $1.37 \cdot 10^{-4}$.

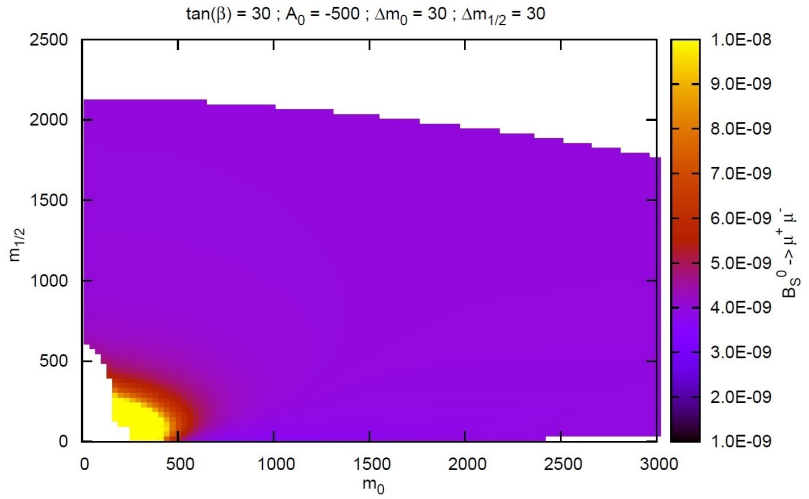

Figure 5: $B_S^0 \longrightarrow \mu^+\mu^-$ for fixed $\tan(\beta) = 30$ and $A_0 = -500$ and fixed steps for m_0 and $m_{1/2}$.

Fig. 5 shows the calculated branching ratio of the $B_S^0 \longrightarrow \mu^+\mu^-$ decay for $\tan(\beta) = 30$ and $A_0 = -500$ and steps of 30 GeV for m_0 and $m_{1/2}$ from 30 to 3000 GeV. Beginning from small m_0 and $m_{1/2}$ the branching ratio decreases until m_0 around 450 GeV and $m_{1/2}$ around 650 GeV. From this on the branching ratio remains nearly constant. The same as said above is valid for this branching ratio, great loop contributions for low m_0 and $m_{1/2}$, while the contributions decrease for high m_0 and $m_{1/2}$. The expected upper limit for $B_S^0 \longrightarrow \mu^+\mu^-$ is $(4.5 \pm 0.2) \cdot 10^{-9}$. Except the for the red to yellow region in the lower left corner the rest of Fig. 5 fulfils this condition.

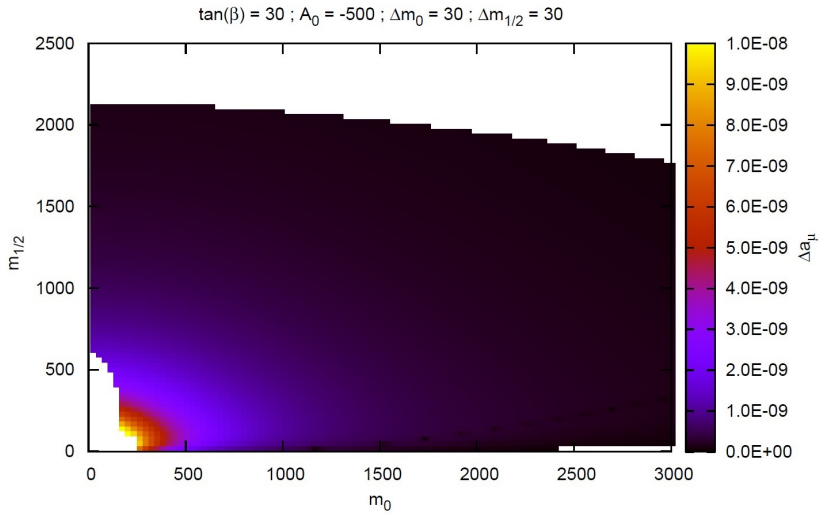

Figure 6: Δa_μ for fixed $\tan(\beta) = 30$ and $A_0 = -500$ and fixed steps for m_0 and $m_{1/2}$.

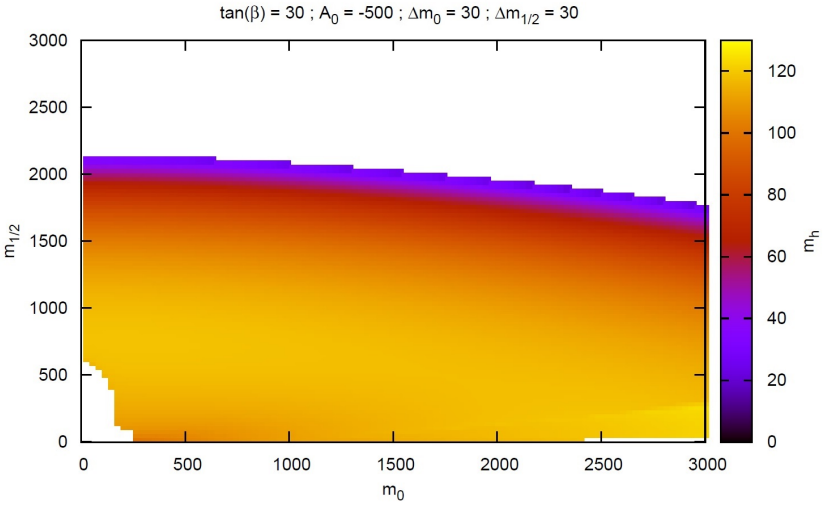

Figure 7: m_h for fixed $\tan(\beta) = 30$ and $A_0 = -500$ and fixed steps for m_0 and $m_{1/2}$.

Fig. 6 shows the calculated anomalous magnetic moment of the muon Δa_μ for $\tan(\beta) = 30$ and $A_0 = -500$ and steps of 30 GeV for m_0 and $m_{1/2}$ from 30 to 3000 GeV. Beginning from small m_0 and $m_{1/2}$ Δa_μ decreases until m_0

around 500 GeV and $m_{1/2}$ around 500 GeV. It matches with the expectation that the SUSY contribution should be great for small m_0 and $m_{1/2}$ and should decrease for higher m_0 and $m_{1/2}$. From then on Δa_μ is still decreasing but rather slightly there before. The expected value $\Delta a_\mu = (3.02 \pm 1.24) \cdot 10^{-9}$ is represented by the slightly violet region in Fig. 6 on the edge to the red region in the lower left corner($m_0 < 750$ GeV, $m_{1/2} < 550$ GeV).

Fig. 7 shows the calculated Higgs mass m_h for $\tan(\beta) = 30$ and $A_0 = -500$ and steps of 30 GeV for m_0 and $m_{1/2}$ from 30 to 3000 GeV. There is just a slight increase of the Higgs mass m_h with m_0. For increasing $m_{1/2}$ the Higgs mass increases to a maximum around 500-600 GeV and decreases from there on. Which matches with the expected behaviour described by Eq. 3. The expected lower limit for m_h is $(114.4 \pm .05)$ GeV. The yellow region in Fig. 7 from $m_{1/2} < 1200$ GeV for $m_0 = 30$ GeV to $m_{1/2} < 600$ GeV for $m_0 = 3000$ GeV fulfils this condition.

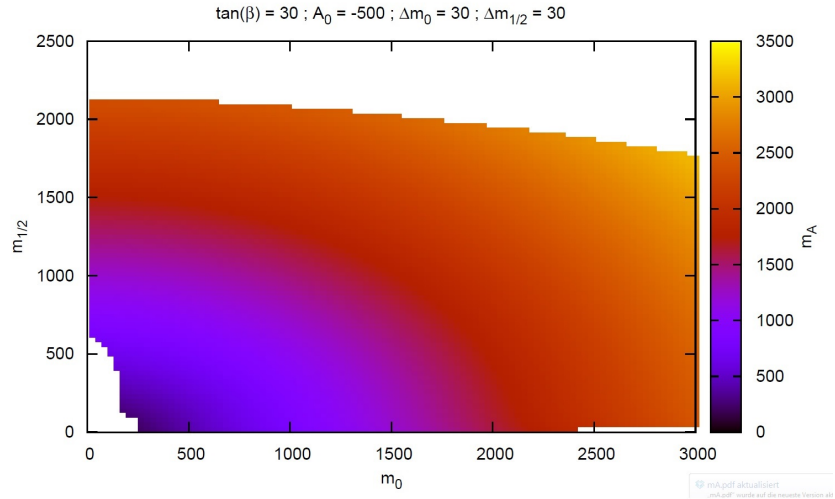

Figure 8: m_A for fixed $\tan(\beta) = 30$ and $A_0 = -500$ and fixed steps for m_0 and $m_{1/2}$.

Fig. 8 shows the calculated pseudo-scalar Higgs mass m_A for $\tan(\beta) = 30$ and $A_0 = -500$ and steps of 30 GeV for m_0 and $m_{1/2}$ from 30 to 3000 GeV. The pseudo-scalar Higgs mass m_A increases, as expected, for increasing m_0 and $m_{1/2}$. The increase of m_A with $m_{1/2}$ is a bit stronger than the increase with m_0. The expected lower limit for m_A is (480 ± 50) GeV. This condition is fulfilled for the nearly whole plot in Fig. 8 except for a small dark violet region for m_0 and $m_{1/2}$ below 500 GeV.

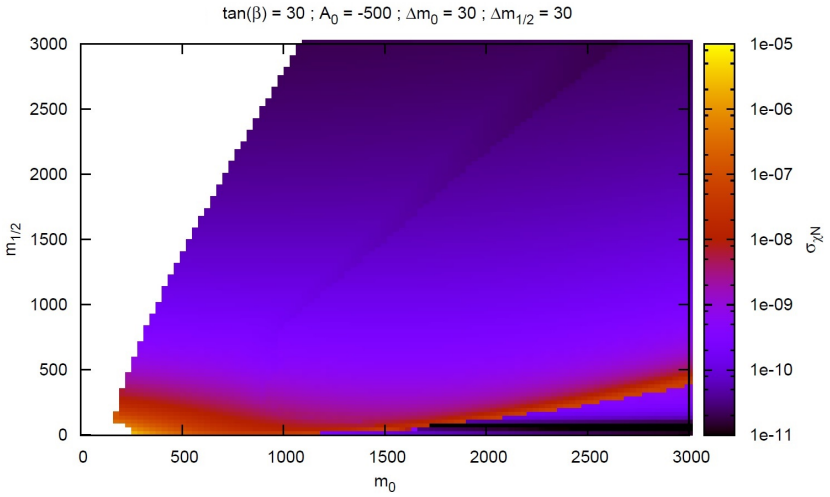

Figure 9: $\sigma_{\chi N}$ for fixed $\tan(\beta) = 30$ and $A_0 = -500$ and fixed steps for m_0 and $m_{1/2}$.

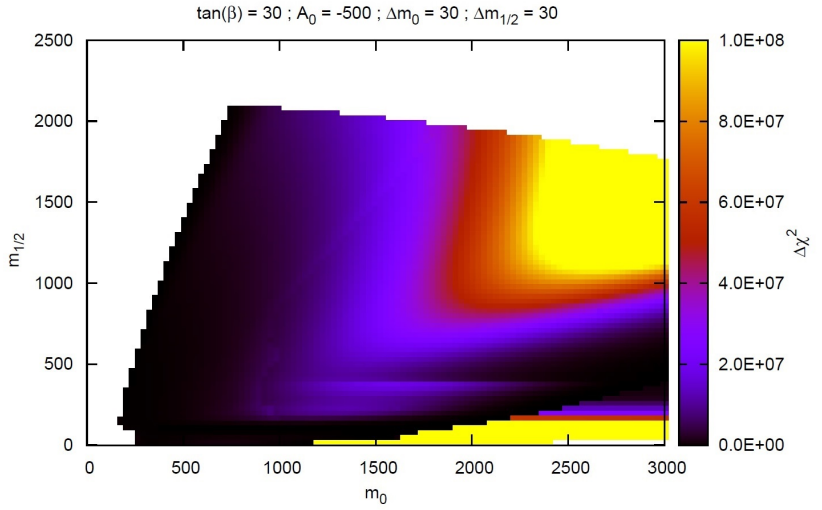

Figure 10: $\Delta\chi^2$ for fixed $\tan(\beta) = 30$ and $A_0 = -500$ and fixed steps for m_0 and $m_{1/2}$.

Fig. 9 shows the calculated cold dark matter nucleon cross section $\sigma_{\chi N}$ for $\tan(\beta) = 30$ and $A_0 = -500$ and steps of 30 GeV for m_0 and $m_{1/2}$ from 30 to 3000 GeV. The cross section increases with increasing $m_{1/2}$, except for the

region in the lower right corner for high m_0 and small $m_{1/2}$. The first matches with the expectations from Fig.5 in Ref.[19], where the cross section is high for small WIMP is much higher, but than the Fig. shown a decrease followed by a slight increase. The expected upper limit for $\sigma_{\chi N}$ is $(2 \pm 1) \cdot 10^{-8}$ pb. This condition is fulfilled for nearly the whole plot in Fig. 9 except for the small dark orange to yellow region for $m_{1/2}$ below 500 GeV.

Fig. 10 shows the deviation from the minimal χ^2 for $\tan(\beta) = 30$ and $A_0 = -500$ and steps of 30 GeV for m_0 and $m_{1/2}$ from 30 to 3000 GeV. The regions of a low deviation from the minimal χ^2 are similar to the region of the Ωh^2 constraint in Fig. 2. The mimimum in Fig. 10 is at $m_0 = 270$ GeV and $m_{1/2} = 570$ GeV. One can see that Fig. 2 and 10 are roughly of the same shape, therefore it seems to be that Ωh^2 has a great influence on $\Delta\chi^2$.

Discussion

The relic density constraint is fulfilled near the charged LSP region and for low $m_{1/2}$. The $b \longrightarrow X_s\gamma$ constraint is fulfilled for a small region for small masses around 200 to 300 GeV. The branching ratio of the $B_u \longrightarrow \tau\nu$ is slightly to low for a great area for masses above around 600 GeV, but there is no region where the constraint is really fulfilled. Since the $B_S^0 \longrightarrow \mu^+\mu^-$ is just an upper limit only a small region for small masses below around 700 GeV has to be excluded, while the rest of the plane fulfils this constraint. Both Higgs masses are lower limits. For the Higgs mass m_h the constraint is fulfilled for m_0 between around 400 and 1200 GeV, while the pseudo-scalar Higgs mass m_A is fulfilled for the whole plane except a region for masses below around 600 GeV. The deviation $\Delta\chi^2$ of the minimal χ^2 has a minimum at $m_0 = 270$ GeV and $m_{1/2} = 570$ GeV. The region of a small deviation are similar to the region which fulfil the relic density constraint. Of course one has to be careful since some of the constraints are just upper or lower limits and are therefore able to be fulfilled even if the deviation is rather large.

3.4 Computation via Markov Chain...

3.4.1 ...for m_0 and $m_{1/2}$ for fixed $\tan(\beta)$ and A_0

All calculations are done for $\mu > 0$. This choice is motivated by the anomalous magnetic moment of the muon[26]. Fig. 11 to 18 show the calculations of the individual constraints via a Markov Chain m_0 and $m_{1/2}$, for $\tan(\beta) = 30$ and $A_0 = -500$ and $m_0, m_{1/2} \in [30\,\text{GeV}, 3000\,\text{GeV}]$. The likelihood function is defined as:

$$L(\chi^2) = \exp(\chi^2/2), \tag{6}$$

where χ^2 is defined analogous to 3.2 as:

$$\chi^2 = \left(\frac{\alpha_{\text{calc}} - \alpha_{\text{exp}}}{\sigma_\alpha} \right)^2, \tag{7}$$

where α_{calc} is the calculated value, α_{exp} is the expected value and σ_α the uncertainty of the contraint α.

One has to be careful since this algorithm leads only to values which are somehow near the constraint, hence some region which are shown in the Figs. 2 to 9 might be missing even if they would fulfil the condition of being higher (lower)vthan the lower (upper) limit(e.g. compare Fig. 8 and Fig. 17).

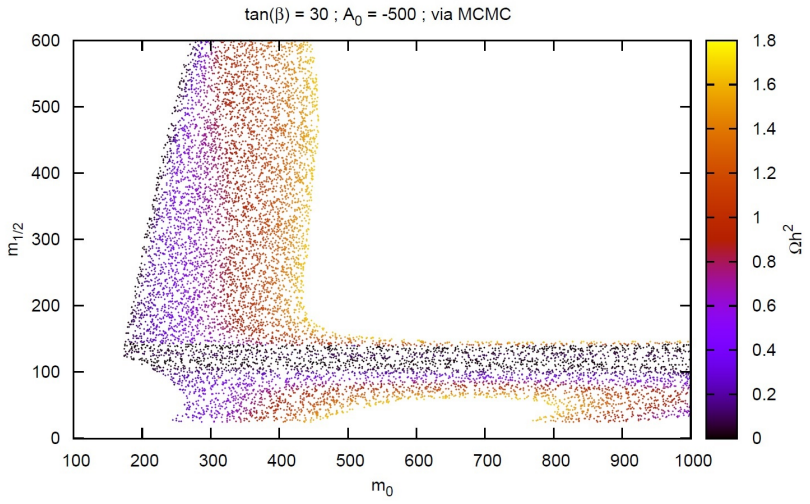

Figure 11: Ωh^2 for fixed $\tan(\beta) = 30$ and $A_0 = -500$ via Markov Chain for m_0 and $m_{1/2}$.

Fig.11 shows the calculated relic density Ωh^2 via a Markov Chain for m_0 and $m_{1/2}$ and $\tan(\beta) = 30$ and $A_0 = -500$. Compared to Fig. 2 a huge region of to high Ωh^2 is excluded by the algorithm. The resulting values are between 0 an 1.8 and are therefore close the expected value of (0.113 ± 0.004). The expected value is represented by the nearly black dots on the edge of the charged LSP region in the upper left corner and for values of m_0 between around 100 and 140 GeV and $m_{1/2}$ between around 180 GeV to 1000 GeV.

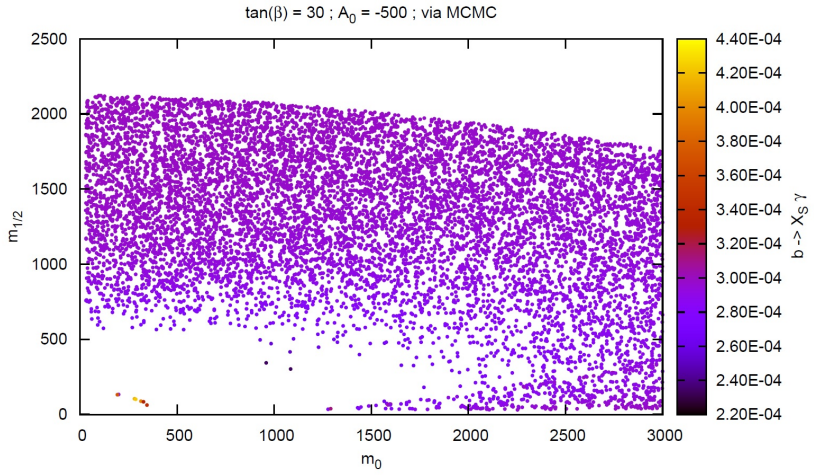

Figure 12: $b \longrightarrow X_S\gamma$ for $\tan(\beta) = 30$ and $A_0 = -500$ via Markov Chain for m_0 and $m_{1/2}$.

Fig.12 shows the calculated branching ratio of the $b \longrightarrow X_S\gamma$ decay via a Markov Chain for m_0 and $m_{1/2}$ and $\tan(\beta) = 30$ and $A_0 = -500$. Fig. 12 looks similar to Fig. 3 on can see just a few points(red to orange) in the lower left corner which fulfil the constraint $b \longrightarrow X_S\gamma = (3.55 \pm 0.24) \cdot 10^{-4}$ and a lot of violet points which are close the constraint but do not fulfil it.

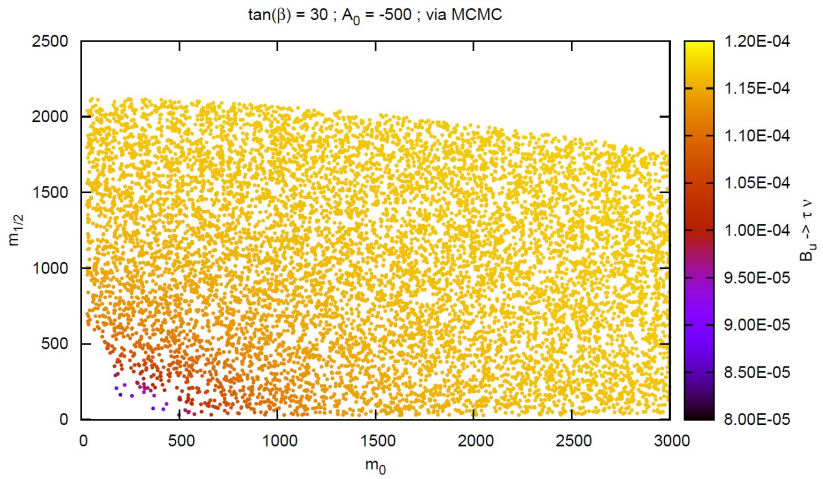

Figure 13: $B_u \longrightarrow \tau\nu$ for $\tan(\beta) = 30$ and $A_0 = -500$ via Markov Chain for m_0 and $m_{1/2}$.

Fig.13 shows the calculated branching ratio of the $B_u \longrightarrow \tau\nu$ decay via a Markov Chain for m_0 and $m_{1/2}$ and $\tan(\beta) = 30$ and $A_0 = -500$. Fig. 13 looks similar to Fig. 4 which is due to the fact that the whole plot does not fulfil the constraint $B_u \longrightarrow \tau\nu = (1.68 \pm 0.31) \cdot 10^{-4}$, but is close to it.

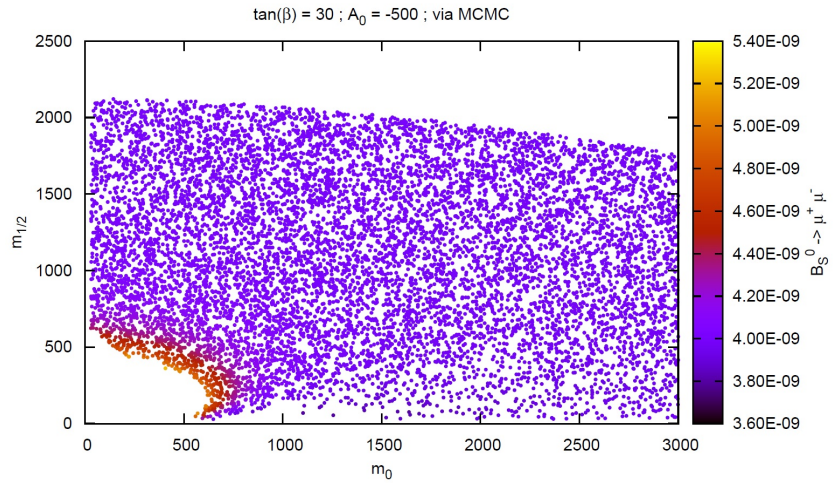

Figure 14: $B_S^0 \longrightarrow \mu^+\mu^-$ for $\tan(\beta) = 30$ and $A_0 = -500$ via Markov Chain for m_0 and $m_{1/2}$.

Fig.14 shows the calculated branching ratio of the $B_S^0 \longrightarrow \mu^+\mu^-$ decay via a Markov Chain for m_0 and $m_{1/2}$ and $\tan(\beta) = 30$ and $A_0 = -500$. Fig. Fig. 14 is similar to Fig. 5 except that the region in the lower left corner which does not fulfil the constraint $B_S^0 \longrightarrow \mu^+\mu^- < (4.5 \pm 0.2) \cdot 10^{-9}$ is excluded by the Markov Chain.

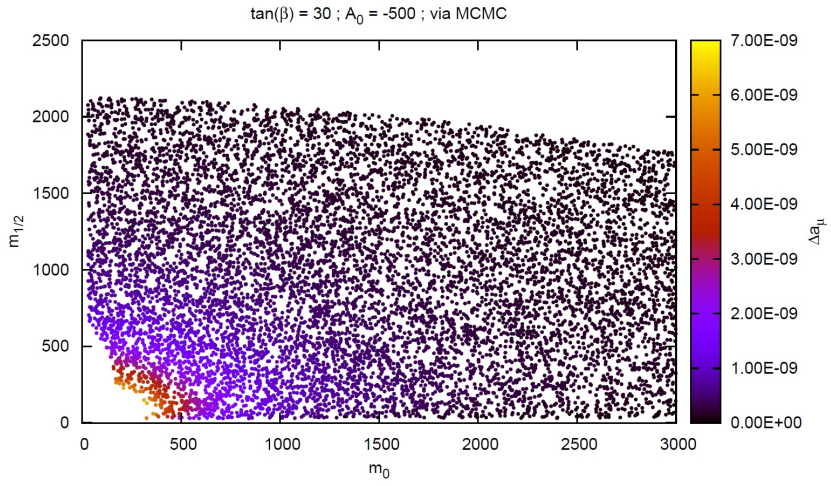

Figure 15: Δa_μ for $\tan(\beta) = 30$ and $A_0 = -500$ via Markov Chain for m_0 and $m_{1/2}$.

Fig.15 shows the calculated anomalous magnetic moment of the muon Δa_μ via a Markov Chain for m_0 and $m_{1/2}$ and $\tan(\beta) = 30$ and $A_0 = -500$. Fig. 15 is similar to Fig. 6 except that the region in the lower left corner which does not fulfil the constraint $\Delta a_\mu = (3.02 \pm 1.24) \cdot 10^{-9}$ is excluded by the Markov Chain.

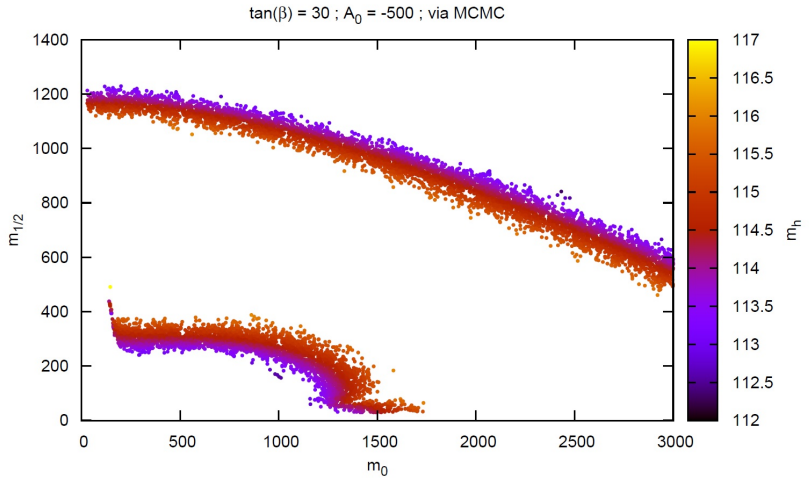

Figure 16: m_h for $\tan(\beta) = 30$ and $A_0 = -500$ via Markov Chain for m_0 and $m_{1/2}$.

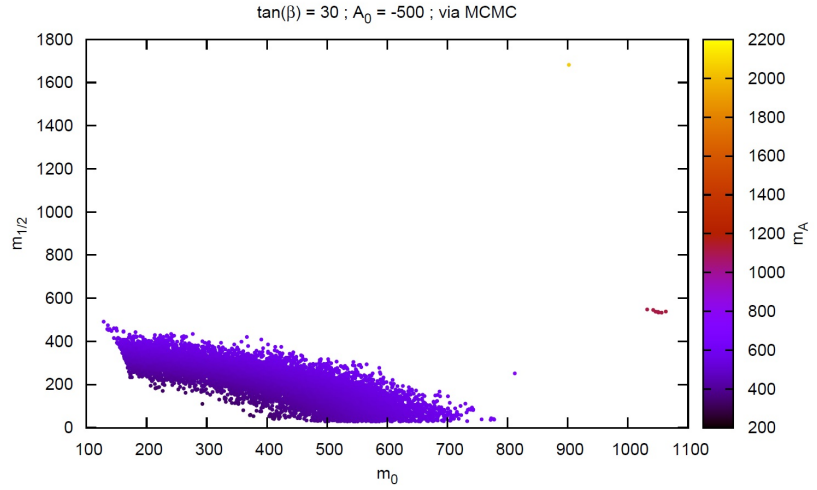

Figure 17: m_A for $\tan(\beta) = 30$ and $A_0 = -500$ via Markov Chain for m_0 and $m_{1/2}$.

Fig.16 shows the calculated Higgs mass m_h via a Markov Chain for m_0 and $m_{1/2}$ and $\tan(\beta) = 30$ and $A_0 = -500$. Fig. 16 is different from Fig. 7 since a part of the area which fulfils the constraint $m_h < (114.4 \pm 0.5)$. Since the Markov Chain only leads to value near the value of $m_h = (114.4 \pm 0.5)$, which

only vary between around 113 and 116 GeV. That there a two regions which fulfil the constraint is due the fact that the Higgs mass first increases to a maximum and then decreases again.

Fig.17 shows the calculated pseudo-scalar Higgs mass m_A via a Markov Chain for m_0 and $m_{1/2}$ and $\tan(\beta) = 30$ and $A_0 = -500$. Fig. 17 is different from Fig. 8 since a part of the area which fulfils the constraint $m_h < (480 \pm 50)$. Since the Markov Chain only leads to value near the value of $m_h = (480 \pm 50)$. But there is one yellow point around 2100 GeV and a few for around 1200 GeV for m_A, which might be a result of the beginning Markov Chain and the search for a high likelihood. But the majority of the acquired points are around 300 to 600 GeV.

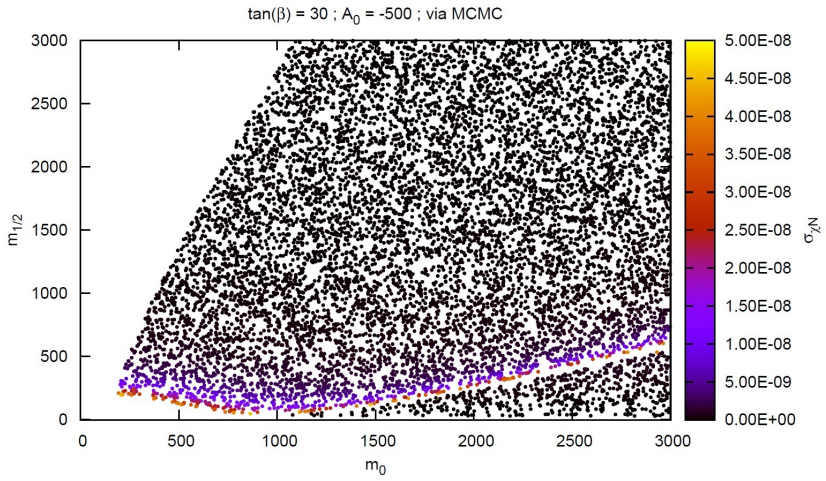

Figure 18: $\sigma_{\chi N}$ for $\tan(\beta) = 30$ and $A_0 = -500$ via Markov Chain for m_0 and $m_{1/2}$.

Fig. 18 shows the calculated cold dark matter nucleon cross section $\sigma_{\chi N}$ via a Markov Chain for m_0 and $m_{1/2}$ and $\tan(\beta) = 30$ and $A_0 = -500$. Fig. 18 is similar to 9 except that the region, which does not fulfil the constraint $\sigma_{\chi N} < (2 \pm 1) \cdot 10^{-8}$ pb, is excluded by the Markov Chain, while the rest of the plot which fulfils the constraint or is at least near the constraint.

A plot similar to Fig. 10 could not be calculated since the used program could not find a valid starting point for the combined constraints. This is due to the fact that, if one uses χ^2 as it is defined in 3.2, the likelihood function seems to be always zero.

Discussion

The plots generated via Markov Chain calculations match(except some exclusions) with the plots of the previous section but since the constraints tend to be fulfilled in rather different region of the mass plane a Monte Carlo calculation with this simple algorithm was not successful. But since the results for the single constraints are quite good and the combined constraints behave similar to the relic density, it seems to be a quite good idea to take a closer look at the relic density with Markov Chain for all four parameters.

3.4.2 ...for m_0, $m_{1/2}$, $\tan(\beta)$ and A_0

All calculations are done for $\mu > 0$. This choice is motivated by the anomalous magnetic moment of the muon[26]. Fig. 11 to 18 show the calculations of the individual constraints via a Markov Chain m_0, $m_{1/2}$, $\tan(\beta)$ and A_0, for m_0, $m_{1/2} \in [30\,\text{GeV}, 3000\,\text{GeV}]$, $\tan(\beta) \in [10, 60]$ and $A_0 \in [-2000, 2000]$. The likelihood function was choosen as:

$$L(\chi^2) = \exp(\chi^2/2), \tag{8}$$

where χ^2 is defined analogous to Ref. [7] as:

$$\chi^2 = \left(\frac{\ln(\Omega h^2_{\text{calc}} / \Omega h^2_{\text{exp}})}{\sigma_{\Omega h^2}} \right)^2, \tag{9}$$

where Ωh^2_{calc} is the calculated relic density, Ωh^2_{exp} is the expected relic density and $\sigma_{\Omega h^2}$ the uncertainty of the expected relic density Ωh^2.

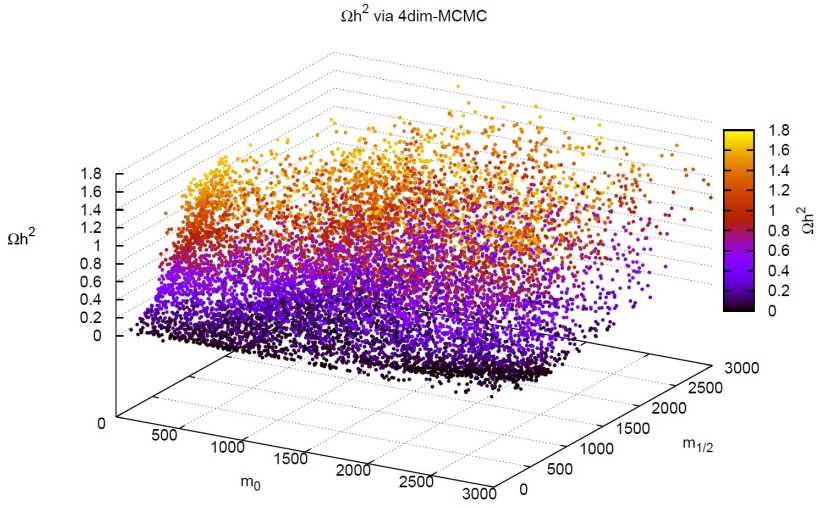

Figure 19: Ωh^2 via Markov Chain for m_0, $m_{1/2}$, $\tan(\beta)$ and A_0
Ωh^2 as color scale.

Fig. 19 shows Ωh^2 on the z-axis and the color scale. This plot shows a Markov Chain of 10000 accepted points for all four parameters.

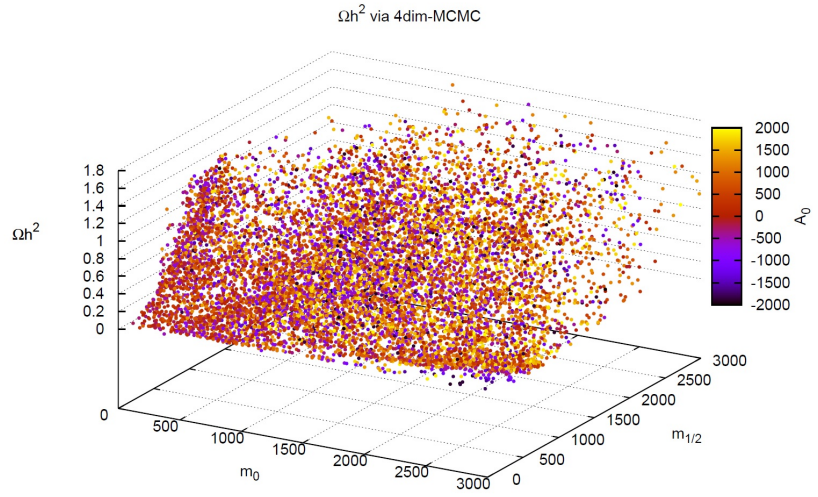

Figure 20: Ωh^2 via Markov Chain for m_0, $m_{1/2}$, $\tan(\beta)$ and A_0
A_0 as color scale.

Fig. 20 shows the same results as 19 but with Ωh^2 on the z-axis and A_0 on the color scale.

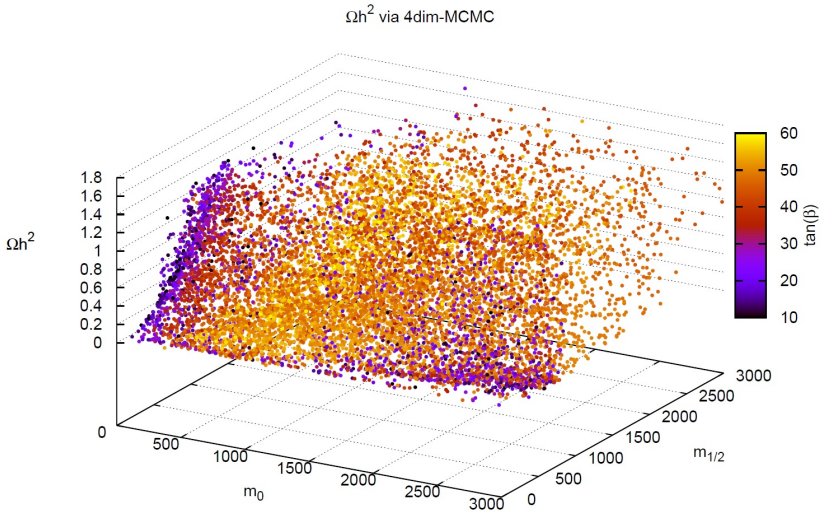

Figure 21: Ωh^2 via Markov Chain for m_0, $m_{1/2}$, $\tan(\beta)$ and A_0
$\tan(\beta)$ as color scale.

Fig. 21 shows the same results as two previous plots but with Ωh^2 on the z-axis and $\tan(\beta)$ on the color scale.

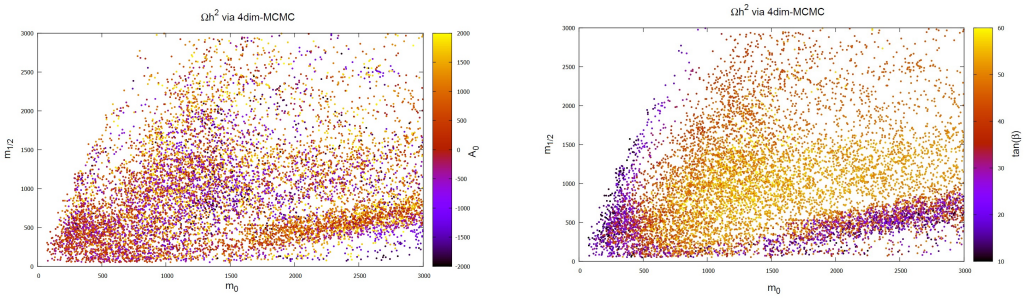

Figure 22: Projection in the m_0, $m_{1/2}$-plane of Fig. 20 (left) and 21 (right).

Fig. 19 to 21 are somehow confusing, therefore Fig. 22 shows the projections of 20 (left) and 21 (right) in the m_0, $m_{1/2}$-plane and only a short quanlitative discussion will be done for this one. Since the expected value is $\Omega h^2 = (0.114 \pm 0.004)$ (see Tab. 6), one can say that the results are quite good, since the calculated values for Ωh^2 lie between 0 and 1.8 for various combination of the four parameters. Furthermore A_0 seems to have a slight tendency for greater absolute values of A_0 for greater values of m_0 and $m_{1/2}$. $\tan(\beta)$ seems to be lower for low values of m_0 **or** $m_{1/2}$ and higher for middle and high values for m_0 **and** $m_{1/2}$.

The Figs. 23 to 25 show an extract of the Figs. 19 to 21 for $\Omega h^2 \in [0.109, 0.117]$ as projections in the m_0, $m_{1/2}$-plane. The Figs. 23 to 25 contain 93 pairs of parameters which would fit the constraint that Ωh^2 has to be in the intervall $[0.109, 0.117]$ with a simple Markov Chain Monte-Carlo algorithm.

By comparing Figs. 23, 24 and 25 one achieves a few points in the parameter space whose parameter sets would fulfil the relic density constraints. As one can see for high values of $\tan(\beta)$ the constraint can be fulfilled even for high masses.

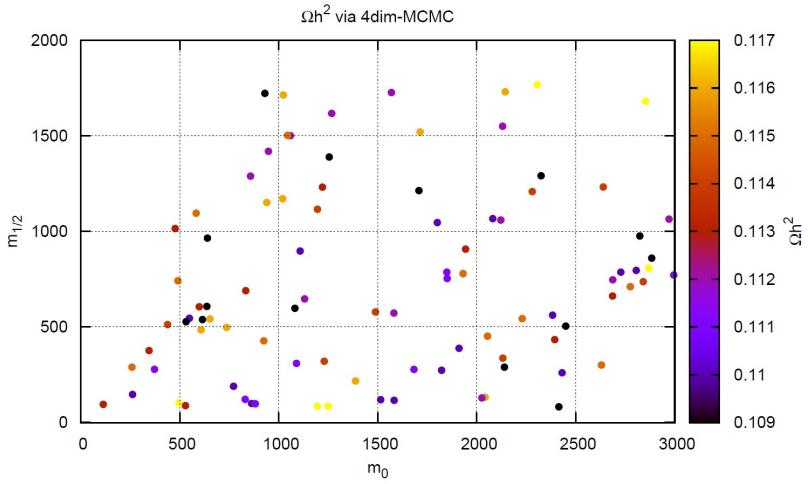

Figure 23: Ωh^2 via Markov Chain for m_0, $m_{1/2}$, $\tan(\beta)$ and A_0
For $\Omega h^2 \in [0.109, 0.117]$, Ωh^2 as color scale.

Fig. 23 shows an extract of Fig. 19, as an projection in the m_0, $m_{1/2}$-plane for $\Omega h^2 \in [0.109, 0.117]$, with Ωh^2 on the color scale.

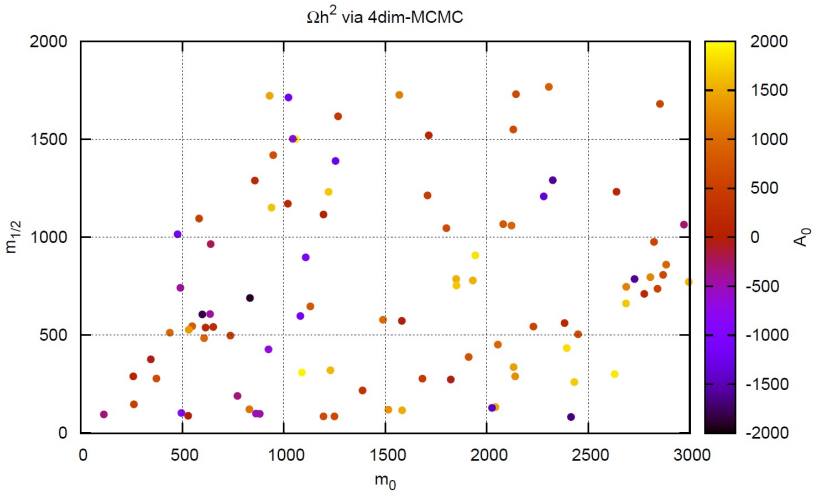

Figure 24: Ωh^2 via Markov Chain for m_0, $m_{1/2}$, $\tan(\beta)$ and A_0
For $\Omega h^2 \in [0.109, 0.117]$, A_0 as color scale.

Fig. 24 shows an extract of Fig. 20, as an projection in the m_0, $m_{1/2}$-plane for $\Omega h^2 \in [0.109, 0.117]$, with A_0 on the color scale.

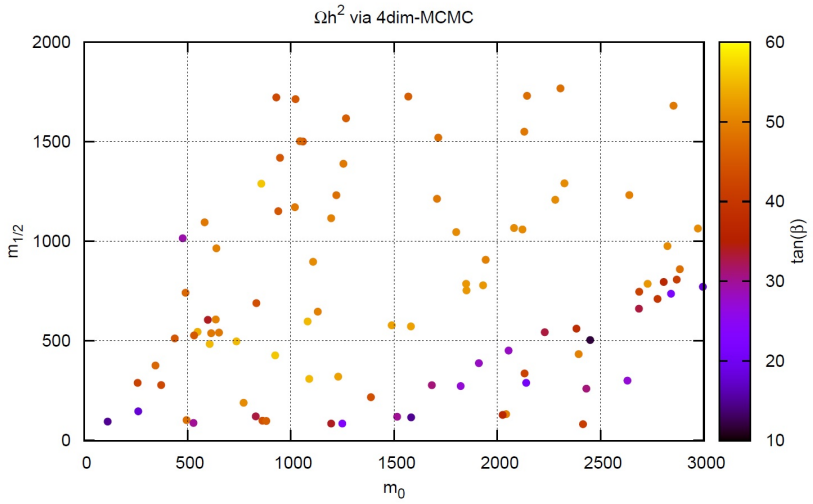

Figure 25: Ωh^2 via Markov Chain for m_0, $m_{1/2}$, $\tan(\beta)$ and A_0
For $\Omega h^2 \in [0.109, 0.117]$, $\tan(\beta)$ as color scale.

Fig. 25 shows an extract of Fig. 21, as an projection in the m_0, $m_{1/2}$-plane for $\Omega h^2 \in [0.109, 0.117]$, with $\tan(\beta)$ on the color scale.

4 Summary and Outlook

Summary

Different constraints are fulfilled in different regions of the m_0, $m_{1/2}$-plane for fixed $\tan(\beta)$ and $A_0 = -500$. The $b \longrightarrow X_S\,\gamma$ constraint is fulfilled for small masses, so does the anomalous magnetic moment of the muon. The $B_u \longrightarrow \tau\,\nu$ and the $B_S^0 \longrightarrow \mu^+, \mu^-$ constraint tend to be fulfilled for middle an high masses. Some for the pseudo-scalar Higgs mass. The Higgs mass contraint is fulfilled for $m_{1/2}$ around 1000 GeV, while m_0 does not have a great influence. The cold dark matter nucleon cross section contraint is fullfilled for $m_{1/2}$ above 500 GeV, while m_0 does not have a great influence. The toughest constraint is the relic density since it is only fulfilled near the charged LSP region respectively for small masses and seems to have a great influence as one can see from the similarity of Fig. 2 and Fig. 10.
The Markov Chain calculations f$\tilde{\text{A}}\frac{1}{4}$r fixed $\tan(\beta)$ and $A_0 = -500$ lead to results which are similir to the fixed step calculation and provide quite good results. The Markov Chain for all four parameters leads to good results. It leads a lot of points near the contraint and even some which fulfil the constraint for very different parameter sets with a rather simple algorithm.

Ideas for further computaion

There are some points that could still could be done, first the dependence of the expected value for the pseudo scalar Higgs mass m_A on $\tan(\beta)$ and the dependence of the cold dark matter nucleon crosssection $\sigma_{\chi N}$ on the LSP mass, which where assumed to be constant during the calculations for reasons of simplicity. Furthermore one could add further constraints, to set close limits the possible regions of the parameter space. Although one could experiment with the likelihood function to get a function which works for a Markov Chain calculation for the combined constraints. Since the Markov Chain calculations for all four parameter are quite good, one should consider to survey more of the constraints via Markov Chain calculations.

References

[1] John F. Donoghue, Eugene Golowich, Barry R. Holstein: Dynamics of the Standard Model, Cambridge University Press, 1994, ISBN 978-0-521-47652-2

[2] R. Alkofer und J. Greensite: Quark Confinement: The Hard Problem of Hadron Physics. In: Journal of Physics. G, Nr. 34, 2007, arXiv:hep-ph/0610365

[3] Stephen P. Martin: A Supersymmetry Primer, September 2011, arXiv:hep-ph/9709356v6

[4] Vera C. Rubin, W. Kent Ford, Jr.: Rotation of the Andromeda Nebula from a Spectroscopic Survey of Emission Regions, In: The Astrophiscal Journal,Vol 159, February 1970

[5] Matts Roos: Introduction to Cosmology, 3. Edition, John Wiley & Sons, Ltd, 2003, ISBN 0-470-84909-6

[6] Virginia Trimble: Existence and Nature of Dark Matter in the Universe. In: Ann.Rev.Astron.Astrophys. 1987.25:425-72

[7] Edward A. Baltz, Paolo Gondolo: Markov Chain Monte Carlo Exploration of Minimal Supergravity with Implications for Dark Matter, July 2004, arXiv:hep-ph/0407039v1

[8] W. Porod, Comput. Phys. Commun. 153 (2003) 275, arXiv:hep-ph/0301101

[9] W. Porod and F. Staub arXiv:1104.1573

[10] G. Bélanger, F. Boudjema, A. Pukhov, A. Semenov, arXiv:hep-ph/1305.0237

[11] C. Beskidt, W. der Boer, D.I. Kazakov, F. Ratnikov: Constraints on supersymmetry from LHC data on SUSY searches and Higgs boson combined with cosmology and direct dark matter searches, arXiv:hep-ph/1207.3185v2

[12] E.Komatsu et al.: Seven-year Wilkinson Microwave Anisotropy Probe (WMAP) observations: cosmological interpretaion, 2011, arXiv:100.4538

[13] https://www.slac.stanford.edu/xorg/hfag/rare/ichep10/radll/OUTPUT/TABLES/radll.pdf, updated August 2010

[14] Muon G-2 Collaboration, Final report of the muon E821 anomalous magnetic moment measurement at BNL, 2006, arXiv:hep-ex/0602035

[15] LHCb collaboration, Strong constraints on the rare decays $B_s \to \mu^+\mu^-$ and $B^0 \to \mu^+\mu^-$, 2012, arXiv:1203.4493

[16] ALEPH Collaboration, DELPHI Collaboration, L3 Collaboration, OPAL Collaborations LEP Working Group for Higgs Boson Searches Collaboration, Search for neutral MSSM Higgs at LEP, 2006, arXiv:hep-ex/0602042

[17] CMS Collaboration, Search for neutral MSSM Higgs bosons decaying to tau tau pairs in pp collisions at sqrt(s) = 7 TeV, 2012, arXiv:121.4083

[18] ATLAS Collaboration, Search for neutral MSSM Higgs bosons decaying into tau tau pairs in proton-proton collision at 7 TeV with ATLAS detector

[19] E Aprile et al., Dark mazzer results from 100 live days if XENON100 data, 2011 arXiv:1104.2549

[20] Koji Ishiwata, Natsumi Nagata, Norimi Yokozaki, Natural Supersymmerty and $b \longrightarrow s\gamma$ constraints, March 2012, arXiv:hep-ph/1112.1944v2

[21] Wolfgang Altmannshofer, Andrzej J. Buras, Stefania Gori, Paride Paradisi, David M. Straub, January 2010, arXiv:hep-ph/0909.1333v2

[22] Björn Herrmann, Michael Klasen, Karol Kovarik, SUSY-QCD effects on neutralino dark matter annihilation beyond scalar or gaugino unification, August 2009, arXiv:0907.0030v2

[23] A. Arbey, M. Battaglia, F. Mahmoudi, D. Martinez Santos, Supersymmetry confronts $B_s \longrightarrow \mu^+\mu^-$:Present and future status, February 2013, arXiv:hep-ph/1212.4887v2

[24] Hideo Itoh, Shinji Komine, Yasuhiro Okada, May 2005, arXiv:hep-ph/0409228v3

[25] Wolfgang Altmannshofer, David M. Straub, Viability of MSSM scenarios oat very large $\tan\beta$, February 2011, arXiv:hep-ph/1004.1993v2

[26] Benjamin Fuks, Michael Klasen, David R. Lamprea, Marcel Rothering, Gaugino production in proton-proton collisions, October 2012, arXiv:hep-ph/12072159v2 at a center-of-mass energy of 8 TeV

Ich versichere hiermit, dass ich meine Bachelorarbeit *Constraints of supersymmetric models with LHC data and direct search for dark matter* selbstständig und ohne fremde Hilfe angefertigt habe, und dass ich alle von anderen Autoren wörtlich übernommenen Stellen, wie auch die sich an die Gedankengänge anderer Autoren eng anlehnenden Ausführungen meiner Arbeit besonders gekennzeichnet und die Quellen zitiert habe.

Münster, den 25. Juli 2013 _____